Article

A Robust Control of Two-Stage Grid-Tied PV Systems Employing Integral Sliding Mode Theory

Abbes Kihal, Fateh Krim *, Talbi Billel, Abdelbaset Laib and Abdeslem Sahli

Laboratory of Power Electronics and Industrial Control (LEPCI), Electronics department, Faculty of technology, University of Sétif1, 19000, Sétif, Algeria; kihalabbas.87@gmail.com (A.K.); bilel_ei@live.fr(B.T.); laib_abdelbaset@univ-setif.dz(A.L.);   sahli_abdeslem@yahoo.fr(A.S.)

* Correspondence: krim_f@ieee.org; Tel.: +213-796-206-432

Abstract: This contribution considers an improved control scheme for three-phase two-stage grid-tied photovoltaic (PV) power system based on integral sliding mode control (ISMC) theory. The proposed control scheme consists of maximum power point tracking (MPPT), DC-Link voltage regulation and grid currents synchronization. A modified voltage-oriented maximum power point tracking (VO-MPPT) method based on ISMC theory is proposed for design of an enhanced MPPT under irradiation changes. Moreover, a novel DC-Link voltage control based on ISMC theory is proposed in order to achieve good regulation of DC-Link voltage over its reference. To inject the generated PV power into the grid with high quality, a voltage oriented control based on space vector modulation (SVM) and ISMC (VOC-ISMC-SVM) has been developed to control the grid currents synchronization. Numerical simulations are performed in Matlab/Simulink™ environment in order to evaluate the proposed control strategy. In comparison with conventional control scheme, the developed control strategy provides an accurate MPP tracking with less power oscillation as well as a fast and an accurate DC-Link regulation under climatic conditions variations. Moreover, the transfer of the extracted power into the grid is achieved with high quality.

Keywords: grid-tied photovoltaic system; maximum power point tracking (MPPT); voltage oriented control (VOC); integral sliding mode control (ISMC)theory; dc-link control.

1. Introduction

In recent years, PV power technology is considered as an important and promising source of energy due to its several advantages such as cleanness, renewability and non-noisy nature [1,2]. To make PV power available for public use, two main topologies are used to transfer the produced PV power into the grid which are called single and two stages [3]. The latter topology has been extensively employed due to the fact that, the MPPT and control of generated power transfer into the grid are decoupled by different converters. This feature offers an easier and better control than the single stage topology control [4,5]. In order to enhance the cost-effectiveness of this topology, the MPP should be tracked quickly and accurately under irradiation changes. Moreover, the DC-Link voltage and power injected into the grid must also be controlled accurately.

Many MPPT techniques have been proposed in the literature to push PV arrays to deliver the maximum possible power under climatic condition changes [6-23]. Perturb and observe (P&O) [7,8] and Incremental Conductance (INC) [9-11] are two well-known conventional MPPT techniques. They are intuitive to understand and easy to be implemented. However, they are not being able to operate properly in case of fast changes in environmental conditions; afterwards, they present large

oscillations at the maximum power point (MPP) in steady-state. In this context, artificial intelligence is adopted to overcome these drawbacks in the form of different methods such as, neural networks [12,13], fuzzy logic [14,15], Genetic Algorithms (GA) [16], Pattern Swarm Optimization (PSO) [17], and Grey Wolf Optimization (GWO) [18]. Unlike the conventional methods, the modern algorithms provide better performance. However, they are complex in design and rigorous to be implemented in practice. Therefore, several research works were interested on Voltage- Oriented MPPT (VO-MPPT) and Current-Oriented MPPT (CO-MPPT) [19-24]. These methods involve MPPT voltage-based algorithm (V-MPPT) in cascade with voltage control loop or MPPT current-based algorithm (I-MPPT) in cascade with current control loop. Due to the almost no change in PV voltage at the MPP under irradiation changes, VO-MPPT is considered as a fast MPP tracking [19,20]. However, the efficiency of this method depends on the voltage regulation design.

In order to ensure transfer of produced PV power into the grid, the DC-Link voltage must be regulated to a desired value higher than the grid peak voltage. The mechanism of this regulation is to maintain the DC-Link voltage to its desired value as well as to estimate the reference current "i_d" whatever the PV power produced. For this purpose, a PI or fuzzy controllers are widely used in the literature [24-27]. However PI regulator suffers from long response time and inaccurate regulation under solar irradiation changes. To overcome the inherent difficulties of the PI controller, several types of fuzzy controllers have been proposed [24,25]. These intelligent controllers provide high performance control. However, they lead to high computational burden which reduces drastically their utilization especially in the case of complex systems.

Obviously, the injection of the produced PV power into the grid must be performed with a low total harmonic distortion (THD) for grid currents. For this purpose, numerous research works are interested in direct power control (DPC) [28] and virtual flux direct power control (VF-DPC) [29] based on switching table. These two techniques do not provide high performance control in addition to the switching frequency is variable and not controllable. Otherwise, some researchers have developed distinct control strategies such as hysteresis control [30] or Finite-set predictive control [31]. Despite these strategies provide high performance control but they suffer from incontrollable switching frequency.   Other research works have employed voltage oriented control (VOC) based on PI controllers through pulse width modulation (PWM) or space vector modulation (SVM) [32]. In these strategies, the PI controller weaknesses reduce the power transfer control performance.

Currently, sliding mode control (SMC) theory is widely introduced in power electronics converters control [33-36]. In grid-tied PV systems, SMC is employed for different purposes such as: to modify the voltage control loop of VO-MPPT [22,23], or internal current loop of VOC [36]. The application of SMC offers high control performance in addition to simple experimental implementation [33-37]. However, it suffers from an undesirable effect named chattering. This problem is inevitably caused by the conventional switching function (signum function) which leads to high switching frequency. In order to reduce this phenomenon, numerous research works use the saturation as switching function [22]. In [23,36] the error between the selected variable and its reference has been used as input of switching surface. However, a steady state error (SSE) still remains. That is why an advanced theory in SMC was developed to enhance the SMC control performance and reduce its disadvantage by adding an integral term to the sliding surface which is called ISMC.

In this paper, ISMC theory is used to develop an effective and simple to implement controller for two-stage grid-tied PV system. Moreover, the control law design has been modified, where an approximation of sign function is used as switching function resulting in a significant reduction of the chattering phenomenon. Firstly, a fixed frequency VO-MPPT based on ISMC theory is proposed to control the first stage and achieve a fast and accurate PV voltage control under solar irradiation changes. Then, a new design of DC-Link voltage control based on ISMC theory is proposed to improve the dynamic performance and tracking compared to other controller types, in the case of linear changes in solar irradiation. Furthermore, to control the injection of produced PV power into the grid with high quality a modified VOC based on ISMC theory is proposed. Furthermore numerical simulations through Matlab/Simulink and Simpower packages are carried out to confirm the improvement in control performance owing to the proposed scheme based on ISMC theory, under solar irradiation changes, in comparison with conventional control scheme based on PI regulator.

Bearing these ideas in mind, the remainder of this paper is arranged as follows. The second section introduces an overview of the global system configuration. The proposed control scheme with detailed procedure design is presented in the third section. Simulation results and discussions are presented in the fourth section, after which conclusions are drawn in the final section.

2. Overall system configuration

The system under consideration which is shown in Figure 1 represents two-stage topology of the grid-tied PV system. It is mainly composed of the following blocks: PV generator (GPV) which converts solar irradiation into electrical energy, DC/DC boost converter is used to track the MPP and deliver it continuously to the DC-Link, two-level three phase inverter whose role is to transfer the generated PV power from the boost converter to the mains grid through a passive filter"R_g, L_g" .
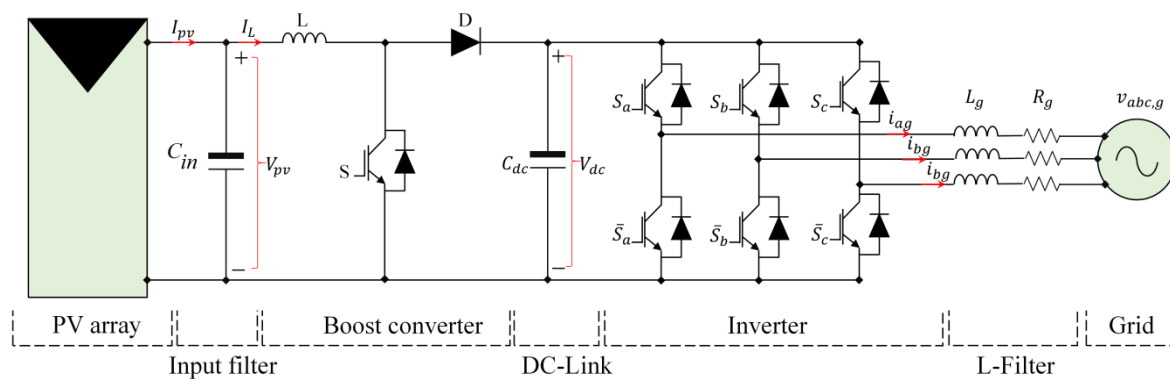

Figure 1. Two-stage grid-tied PV system topology

2.1. PV panel model

The PV cell is the basic component in the conversion of sunlight into direct electrical energy. A number of PV cells connected either in series or parallel form a PV panel which could be modeled by the following equation [6]

$$i_{pv} = N_p i_{ph} - N_p i_o \left[e^{\frac{N_s v_{pv} + (N_s/N_p) R_{sPV} i_{pv}}{a N_s v_t}} - 1 \right] - \frac{N_s v_{pv} + (N_s/N_p) R_{sPV} i_{pv}}{(N_s/N_p) R_{shPV}}, \qquad (1)$$

where, i_{ph} is the photocurrent, i_o the reverse saturation or leakage current of the diode, R_{sPV} and R_{shPV} respectively the series and shunt resistances of the PV cell, v_t the thermal voltage of the PV module, a the diode ideality factor, N_s and N_P the numbers of PV cells in series and parallel respectively [6].

2.2. Boost converter modeling

The boost is a DC-DC converter topology that provides a positive regulated output voltage. It is usually used in PV systems for tracking the MPP produced by the GPV due to some of its important features, such as simplicity, robustness, and continuous input current. Figure 2 shows the equivalent boost circuits for both on and off switching states. The dynamic model of the boost converter in term of duty cycle "D" can be expressed, using averaging method presented in [37], as

$$\begin{cases} \dfrac{dv_{pv}}{dt} = \dfrac{i_{pv} - i_L}{C_{in}} \\ \dfrac{di_L}{dt} = \dfrac{v_{pv} - v_{dc} + Dv_{dc}}{L} \end{cases} \qquad (2)$$

where, i_L and v_{pv} are the state variables; D duty cycle, considered as input variable; v_{dc} the DC-Link capacitor voltage.
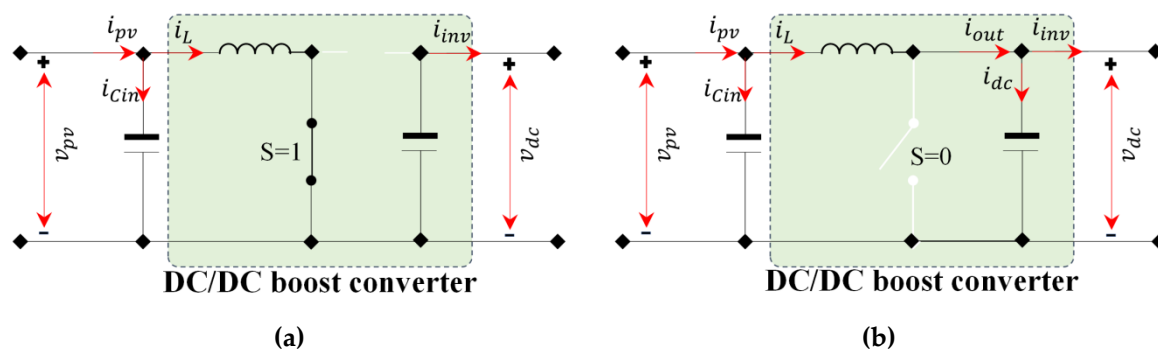

Figure 2. Equivalent boost circuit: (a) on state; (b) off state

2.3. Inverter model

The power circuit of the three-phase inverter consists of six bidirectional switches to connect the three-phase grid directly. Each bidirectional switch is composed of an IGBT with a antiparallel diode. The two switches of each inverter leg must operate in a complementary mode to avoid the short circuit of the DC-Link. The inverter voltage vector can be expressed in terms of DC-Link voltage and switching states as follows [19]:

$$v = v_{dc}\left[\frac{2}{3}\left(S_a + e^{j2\pi/3}S_b + e^{j4\pi/3}S_c \right) \right], \qquad (3)$$

Where; S_a, S_b and S_c are the switching states of the inverter.

3. Proposed Control Scheme

The proposed controllers for two-stage grid-tied PV system are as follows:

- VO-MPPT based on ISMC, to enhance the PV energy conversion efficiency under any irradiation changes.
- DC-Link voltage regulation based on ISMC, to maintain the DC-Link voltage close to its reference under any irradiation changes.
- VOC based on the modified ISMC and SVM, to control the injection of the produced PV power into the grid.

3.1. ISMC theory

The concept of an ISM controller generally includes three steps. The first step concerns the design of a sliding surface on which the sliding motion will take place. The control law is designed in the second step. The control law concept depends on the selection of switching function in order to force the system state trajectories to track and slide on the sliding surface. Whereas, the last step ensures the reaching condition, which pledges the existence of the sliding mode [38,39].

In the present contribution, a high-performance control scheme for grid-tied PV system using ISM controllers is proposed. In ISMC theory, an integral term is added to the sliding surface in order to obtain a high performance control, which means a quick and accurate tracking. The sliding surface "s" in an ISM controller can be expressed as:

$$s = e + k_i \int e \, dt, \tag{4}$$

where, e is the error between the measured variable and its reference, k_i is the sliding surface coefficient.

Typically, the control law has a structure given as;

$$u = u_{eq} + u_{dis}, \tag{5}$$

where, u_{eq} *is* the equivalent part responsible for helping to keep sliding, and u_{dis} is the discontinuous part used to enforce the sliding mode to remain along the sliding surface traditionally written as follows:

$$u_{dis} = -\mathcal{M} \, sign \, (s), \tag{6}$$

where, $\mathcal{M}$ is the proportional gain of discontinuous control and $sign \, (s)$ is sign function.

The discontinuity related with this part leads to chattering phenomenon. To eliminate this drawback, the sign function is replaced with its smoothing approximation, as shown in Figure 3.   Hence u_{dis} can be expressed by the following equation:

$$u_{dis} = -\mathcal{M} \, \frac{s}{\|s\| + \alpha} \tag{7}$$
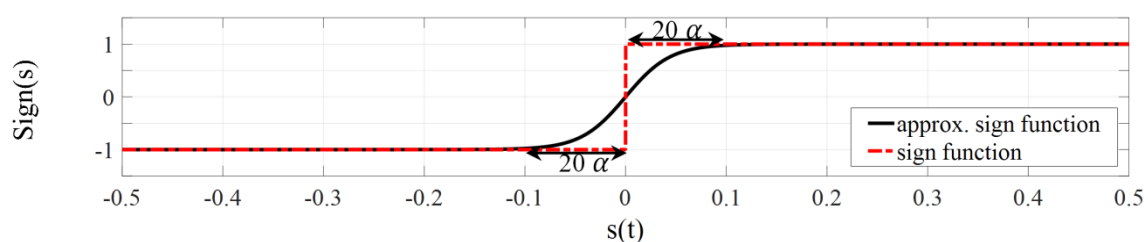
Where, α is a small positive number.

Figure 3. Approximation of sign function

After the control law design in the previous steps, in the next, the conditions required to ensure the control stability will be checked. Firstly, Lyapunov function is utilized to examine the control stability. It is defined as follows;

$$V = \frac{1}{2}s^2 \tag{8}$$

Therefore, to guarantee the convergence of V, it should be verified that the derivative of V is definite negative as follows:

$$\dot{V} = s\dot{s} < 0 \tag{9}$$

Accordingly, one will define individually the reaching condition for each of the three proposed controllers, in the following sections.

3.2. MPPT control

To obtain an optimal exploitation of the GPV during all climatic changes, the proposed control scheme is divided in two steps as shown in Figure 4. Firstly a P&O based voltage V-MPPT generates the reference voltage V_{ref}. After that, an improved ISMC based cascade voltage regulator is proposed to enforce v_{pv} to track V_{ref} generated previously by providing the suitable duty cycle D for PWM operation of the boost converter.
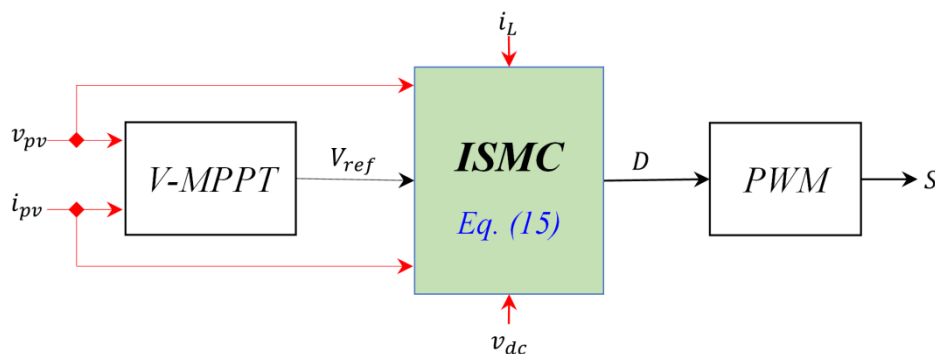
Figure 4. Block diagram of proposed VO-MPPT

3.2.1. P&O based VMPPT

The objective is to generate V_{ref} corresponding to the MPP. For this purpose, P&O based V-MPPT technique is employed due to its featuring effectiveness and simplicity as shown in Figure 5.
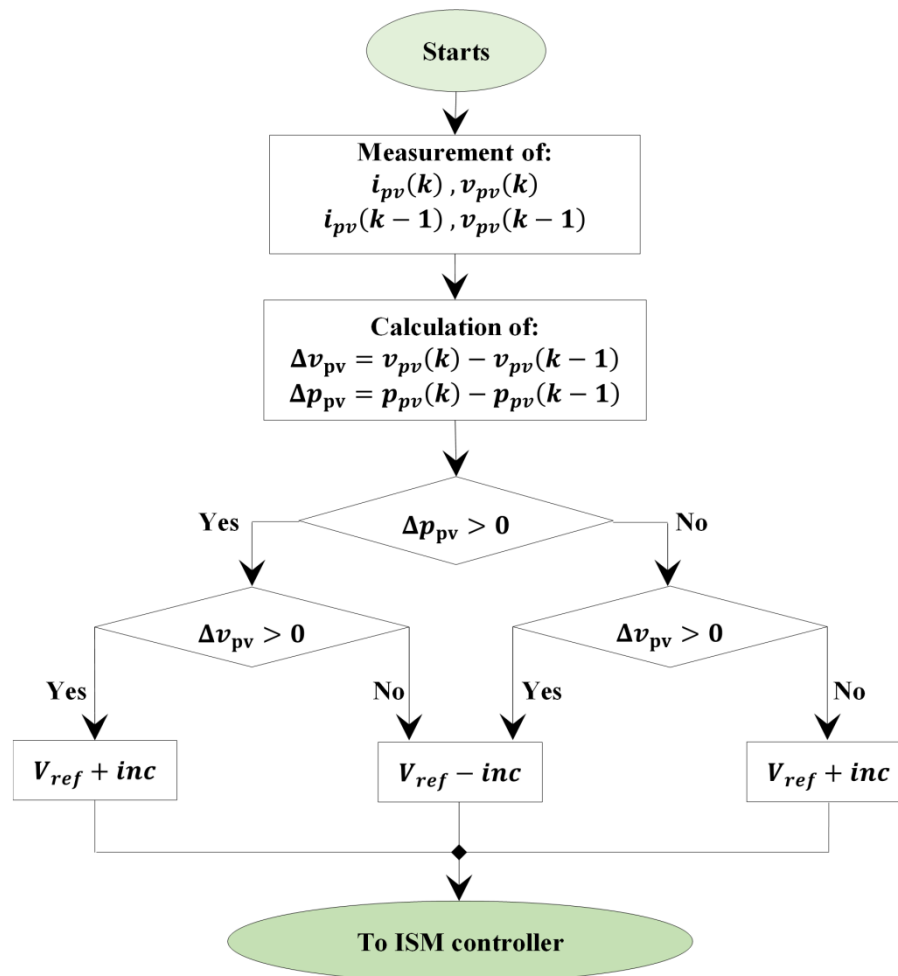
Figure 5. P&O based V-MPPT flowchart

3.2.2. VO-MPPT based on ISMC theory

Due to the nonlinear relationship between the PV voltage and irradiation level, VO-MPPT is considered as a fast alternative [18,19]. However, the efficiency of this method depends on the cascade voltage regulator concept. In this section, an enhanced cascade voltage regulator based on ISMC theory is proposed to provide the suitable duty ratio D to drive the boost converter towards V_{ref} in order to improve the GPV behavior. Hence, in the controller strategy the sliding surface has the same form as given in Equation (4) and expressed as:

$$s_{pv} = e_{pv} + k_{i,PV} \int e_{pv}\ dt, \tag{10}$$

where, $e_{pv}(t)$ is the voltage error between "V_{ref}" and "v_{pv}" and $k_{i,PV}$ is the sliding surface coefficient. It is considered that δ is the sliding surface derivative, which is also called the sliding manifold, given as:

$$\delta = \dot{s}_{pv} = \dot{e}_{pv} + k_{i,PV} e_{pv}, \tag{11}$$

To obtain the equivalent control signal, Equation (11) must be derived and made equal to zero as follows:

$$\dot{\delta} = \ddot{e}_{pv} + k_{i,PV}\dot{e}_{pv} = 0$$
$$\text{or } -\ddot{v}_{pv} - k_{i,PV}\dot{v}_{pv} = 0 \tag{12}$$

By using Equation (2), Equation (12) can be written as:

$$-\frac{\left(\dot{i}_{pv} - \frac{1}{L}\left[v_{pv} - v_{dc} + v_{dc}.D\right]\right)}{C_{in}} - \frac{k_{i,PV}\left[i_{pv} - i_L\right]}{C_{in}} = 0 \tag{13}$$

Thus, the equivalent control can be expressed as:

$$D_{eq} = \frac{\left(v_{dc} - v_{pv} + L.k_{i,PV}\left[i_{pv} - i_L\right] + L.\dot{i}_{pv}\right)}{v_{dc}}, \tag{14}$$

Hence one part of the control input can be obtained; the second part called D_{dis} is given by Equation (7).

Therefore the overall sliding mode controller is expressed as;

$$D = \frac{\left(v_{dc} - v_{pv} + L.k_{i,PV}\left[i_{pv} - i_L\right] + L.\dot{i}_{pv}\right)}{v_{dc}} - \mathcal{M}_{PV}\frac{s_{pv}}{\|s_{pv}\| + \alpha}, \tag{15}$$

where, $\mathcal{M}_{PV}$ is the proportional gain of discontinuous control parts.

The controller described by Equation (15) must satisfy the reaching condition. From Equation (2), we obtain

$$\begin{cases} \dot{v}_{pv} = \dfrac{\left[i_{pv} - i_L\right]}{C_{in}} \\[3mm] \ddot{v}_{pv} = \dfrac{\left[\dot{i}_{pv} - \frac{1}{L}\left[v_{pv} - v_{dc} + Dv_{dc}\right]\right]}{C_{in}} \end{cases} \tag{16}$$

By substituting $\dot{v}_{pv}$ and $\ddot{v}_{pv}$ in Equation (12), we get

$$\dot{\delta} = -\frac{\left[\dot{i}_{pv} - \frac{1}{L}\left[v_{pv} - v_{dc} + Dv_{dc}\right]\right]}{C_{in}} - k_{i,PV}\frac{\left[i_{pv} - i_L\right]}{C_{in}}, \tag{17}$$

By substituting the overall control law D given by Equation (15) in Equation (17) and after some simplifications, we get

$$\dot{\delta} = -\mathcal{M}_{PV}\left(\frac{v_{dc}}{L.C_{in}}\frac{s_{pv}}{\|s_{pv}\| + \alpha}\right), \tag{18}$$

Finally the reaching condition must be verified, which means $\delta.\dot{\delta} < 0$. Thus

$$\delta.\dot{\delta} = \|\delta\|\left\{-\mathcal{M}_{PV}\left(\frac{v_{dc}}{L.C_{in}}\frac{s_{pv}}{\|s_{pv}\| + \alpha}\right)\right\} < 0 \tag{19}$$

Since $\frac{s_{pv}}{\|s_{pv}\| + \alpha}$ and $\frac{v_{dc}}{L.C_{in}}$ are always positive, it is obvious that the reaching condition is verified only if $\mathcal{M}_{PV}$ is chosen positive.

3.3. Design of DC Link voltage controller

As mentioned previously the objective of DC-Link regulation is to maintain the DC-Link voltage close to its reference value and estimate the reference current "i_{dg}^*" whatever the produced PV power. For this purpose, a novel design based on ISMC theory for the DC-Link voltage control is detailed in this section. The block diagram of the proposed DC-Link controller is shown in Figure 6.
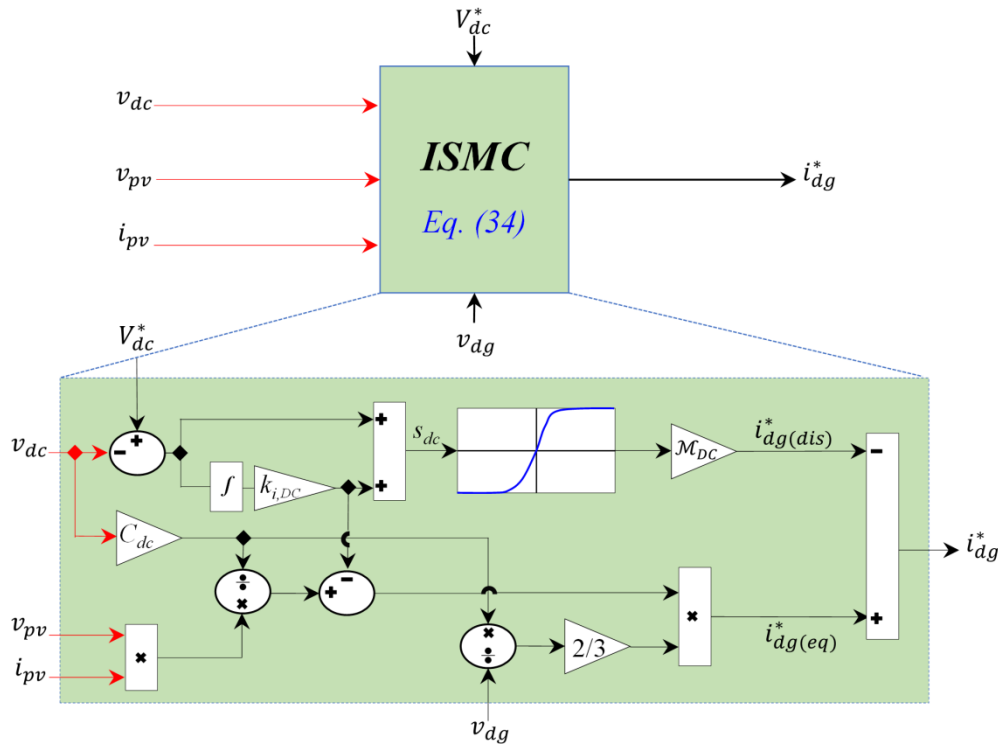

Figure 6. Block diagram of proposed DC-Link ISMC regulator

The proposed sliding surface of the DC-Link voltage control is given below

$$s_{dc} = e_{dc} + k_{i,DC} \int e_{dc} \, dt \,, \tag{20}$$

where, e_{dc} is the voltage error between the DC-Link voltage "v_{dc}" and its reference value "v_{dc-ref}" and $k_{i,DC}$ is the sliding surface coefficient.

The time derivative of the previous equation is given by

$$\dot{s}_{dc} = -\dot{v}_{dc} + k_{i,DC} e_{dc} \,, \tag{21}$$

By considering energy conservation, it yields

$$p_{pv} = p_{dc} = p_g \tag{22}$$

where; p_{pv}, p_{dc} and p_g are the produced PV power, DC-Link power and power injected into the grid respectively.

The injected power into the three phase grid system (in synchronous d-q frame) is expressed as:

$$p_g = \frac{3}{2}\left(v_{dg}\, i_{dg} + v_{qg}\, i_{qg}\right), \tag{23}$$

The aim of the proposed controller is to inject only the produced PV power. According to this condition, p_{qg} becomes null and Equation (23) can be rewritten as

$$p_g = \frac{3}{2}\left(v_{dg}\, i_{dg}\right), \tag{24}$$

The inverter input power is given as:

$$p_{dc} = v_{dc}\, i_{inv}\,, \tag{25}$$

By applying KCL at the DC-Link between the inverter and boost converter it yields

$$i_{dc} = C_{dc}\frac{dv_{dc}}{dt} = (i_{out} - i_{inv})\,,$$

$$\text{or} \qquad \dot{v}_{dc} = \frac{(i_{out} - i_{inv})}{C_{dc}} \tag{26}$$

Where, i_{out} is the boost output current, i_{inv} inverter input current and C_{dc} is the DC-Link capacitor.

By substituting Equation (24) and Equation (25) in Equation (22), it yields

$$v_{dc}\, i_{inv} = \frac{3}{2}\left(v_{dg}\, i_{dg}\right),$$

$$\text{or} \quad i_{inv} = \frac{3v_{dg}}{2v_{dc}}\, i_{dg} \tag{27}$$

By assuming that the DC-Link voltage v_{dc} is properly regulated, the derivative of the DC-Link voltage v_{dc} (or capacitor current i_{dc}) becomes close to zero. Then Equation (26) can be written as

$$i_{inv} = i_{out} \tag{28}$$

Then,

$$p_{dc} = v_{dc}.\,i_{out} = p_{pv} \tag{29}$$

The current i_o can be determined as

$$i_{out} = \frac{p_{pv}}{v_{dc}}\,, \tag{30}$$

By replacing Equation (30) and Equation (27) in Equation (26), we get;

$$\dot{v}_{dc} = \frac{1}{C_{dc}}\left(\frac{p_{pv}}{v_{dc}} - \frac{3v_{dg}}{2v_{dc}}\, i_{dg}\right), \tag{31}$$

To determine the equivalent control, Equation (21) must be set to zero as follows

$$\dot{s}_{dc} = -\dot{v}_{dc}(t) + k_{i,DC}e_{dc}(t) = 0$$

$$\Rightarrow -\frac{1}{C_{dc}}\left(\frac{p_{pv}}{v_{dc}} - \frac{3v_{dg}}{2v_{dc}}\, i_{dg}\right) + k_{i,DC}e_{dc}(t) = 0 \tag{32}$$

From Equation (32) the equivalent control law is expressed as

$$i_{dg(eq)}^* = \frac{2C_{dc}v_{dc}}{3v_{dg}}\left(\frac{p_{pv}}{C_{dc}v_{dc}} - k_{i,DC}e_{dc}(t)\right), \tag{33}$$

Therefore the global control law can be written as

$$i_{dg}^* = \frac{2C_{dc}v_{dc}}{3v_{dg}}\left(\frac{p_{pv}}{C_{dc}v_{dc}} - k_{i,DC}e_{dc}(t)\right) - \mathcal{M}_{DC}\,\frac{s_{dc}}{\|s_{dc}\| + \alpha}, \tag{34}$$

where, $\mathcal{M}_{DC}$ is the proportional gain of discontinuous control part.

To confirm that the controller described by Equation (34) satisfies the reaching condition "$\dot{s}_{dc}$" needs to be evaluated.

By substituting Equation (31) in Equation (21), we get,

$$\dot{s}_{dc} = -\frac{1}{C_{dc}}\left(\frac{p_{pv}}{v_{dc}} - \frac{3v_{dg}}{2v_{dc}}i_{dg}\right) + k_{i,DC}e_{dc}, \tag{35}$$

By substituting the overall control law "i_{dg}^*" given by Equation (34) in Equation (35), we get

$$\dot{s}_{dc} = -\mathcal{M}_{DC}\frac{3v_{dg}}{2C_{dc}v_{dc}}\left(\frac{s_{dc}}{\|s_{dc}\| + \alpha}\right), \tag{36}$$

As previously the condition $s_{dc}.\dot{s}_{dc} < 0$ must be verified. Thus

$$s_{dc}.\dot{s}_{dc} = -\mathcal{M}_{DC}\left\{\frac{3v_{dg}}{2C_{dc}v_{dc}}\,\frac{s_{dc}^{\,2}}{\|s_{dc}\| + \alpha}\right\} < 0 \tag{37}$$

Since $\left(\frac{s_{dc}^{\,2}}{\|s_{dc}\|+\alpha}\right)$ and $\left(\frac{3v_{dg}}{2C_{dc}v_{dc}}\right)$ are positive, so it is clear that the reaching condition is verified only if $\mathcal{M}_{DC}$ is chosen positive.

3.4. VOC based ISMC

In this section, a modified VOC based on ISM control theory (VOC-ISM) is presented and detailed. The main objective of the proposed control scheme is to inject the generated PV power into the grid with high current quality. VOC-ISM is based on the calculation of the reference voltage vector which is applied through SVM in order to minimize the error between the rotating frame current "i_{dg}" , "i_{qg}" and its reference "i_{dg}^*" ,"i_{qg}^*". Figure 7 summarizes the functionality of VOC-ISM. Firstly, "i_{dg}^*" is estimated by the DC-Link voltage regulator mentioned in the above section, while "i_{qg}^*" is set to zero to eliminate the injection of reactive power into the grid. Then, the reference voltage vector$(V_d^*,\ V_q^*)$ obtained, is transformed to α-β frame. Then,$(V_\alpha^*,\ V_\beta^*)$ is applied through SVM to control grid-tied inverter. The phase-locked loop (PLL) provides the synchronization between grid voltages and currents and is also needed for the Park's transformation.
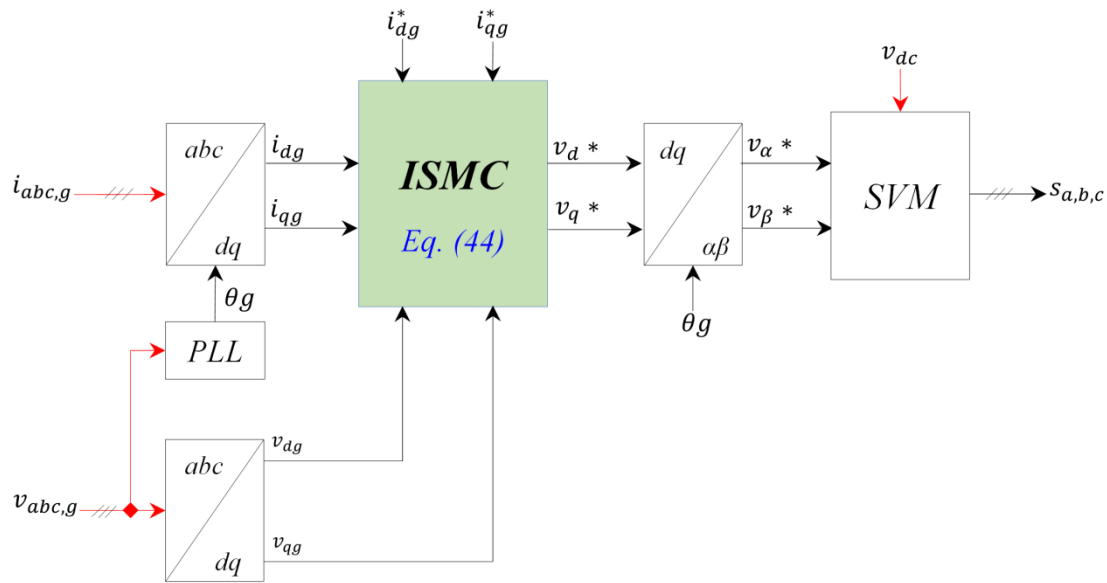
Figure 7. Proposed control scheme for grid-tied PV system

The development of the proposed control scheme needs the mathematical model, the grid-tied inverter model in d-q rotating frame can be described in terms of inverter voltages, grid voltages, and filter inductance presented in [40]   as

$$
\begin{cases}
\dfrac{di_{dg}}{dt} = \dfrac{\left(-R_g i_{dg} - v_{dg} + V_d\right)}{L_g} + \omega i_{qg} \\
\dfrac{di_{qg}}{dt} = \dfrac{\left(-R_g i_{qg} - v_{qg} + V_q\right)}{L_g} - \omega i_{dg}
\end{cases}
\tag{38}
$$

where $(v_{dg}$, $v_{qg})$, $(i_{dg}$, $i_{qg})$ and $(V_d$, $V_q)$ are the (d-q) components of grid voltages, grid currents and inverter output voltages respectively; ω is the grid angular frequency; R_g and L_g are the resistance and inductance of the filter, respectively.

The proposed sliding mode surfaces are defined as follows

$$
\begin{cases}
s_d = e_d + k_{i,d} \displaystyle\int e_d\, dt \\
s_q = e_q + k_{i,q} \displaystyle\int e_q\, dt
\end{cases}
\tag{39}
$$

Where, e_d is the current error between i_{dg}^* and i_{dg} while e_q is the error between i_{qg}^* and i_{qg}; $k_{i,d}$, $k_{i,q}$ are constant gains.

The time derivative of the above equation yields

$$
\begin{cases}
\dot{s}_d = -\dot{i}_{dg} + k_{i,d} e_d \\
\dot{s}_q = -\dot{i}_{qg} + k_{i,q} e_q
\end{cases}
\tag{40}
$$

The equivalent control terms are obtained by setting $\dot{s}_d$ and $\dot{s}_q$ to zero. Thus,

$$
\begin{cases}
\dot{s}_d = -\dot{i}_{dg} + k_{i,d} e_d = 0 \\
\dot{s}_q = -\dot{i}_{qg} + k_{i,q} e_q = 0
\end{cases}
\tag{41}
$$

By using Equation (38), Equation (41) can be expressed as

$$\begin{cases} -\left[\dfrac{(-R_g i_{dg} - v_{dg} + V_d)}{L_g} + \omega i_{qg}\right] + k_{i,d} e_d = 0 \\ -\left[\dfrac{(-R_g i_{qg} - v_{qg} + V_q)}{L_g} - \omega i_{dg}\right] + k_{i,q} e_q = 0 \end{cases} \tag{42}$$

The equivalent control terms are given by

$$\begin{cases} V_{d(eq)} = R_g i_{dg} - \omega L_g i_{qg} + v_{dg} + L_g k_{i,d} e_d \\ V_{q(eq)} = R_g i_{qg} + \omega L_g i_{dg} + v_{qg} + L_g k_{i,q} e_q \end{cases} \tag{43}$$

The global control law is summarized as follows

$$\begin{cases} V_d = R_g i_{dg} - \omega L_g i_{qg} + v_{dg} + L_g k_{i,d} e_d - \mathcal{M}_d \dfrac{s_d}{\|s_d\| + \alpha} \\ V_q = R_g i_{qg} + \omega L_g i_{dg} + v_{qg} + L_g k_{i,q} e_q - \mathcal{M}_q \dfrac{s_q}{\|s_q\| + \alpha} \end{cases} \tag{44}$$

Where, $\mathcal{M}_d$ and $\mathcal{M}_q$ are proportional gains of the discontinuous control parts.

To confirm that the controller described in Equation (44) satisfies the reaching condition, need the expressions of $\dot{s}_d$ and $\dot{s}_q$ are needed.

So by substituting Equation (38) in Equation (40), we get

$$\begin{cases} \dot{s}_d = -\left[\dfrac{(-R_g i_{dg} - v_{dg} + V_d)}{L_g} + \omega i_{qg}\right] + k_{i,d} e_d \\ \dot{s}_q = -\left[\dfrac{(-R_g i_{qg} - v_{qg} + V_q)}{L_g} - \omega i_{dg}\right] + k_{i,q} e_q \end{cases} \tag{45}$$

Then, we replace the global control law (V_d and V_q) given by Equation (44) in Equation (45) to get

$$\begin{cases} \dot{s}_d = \dfrac{\mathcal{M}_d}{L_g} \dfrac{s_d}{\|s_d\| + \alpha} \\ \dot{s}_q = \dfrac{\mathcal{M}_q}{L_g} \dfrac{s_q}{\|s_q\| + \alpha} \end{cases} \tag{46}$$

The reaching condition can be expressed as

$$\begin{cases} s_d \cdot \dot{s}_d < 0 \\ s_q \cdot \dot{s}_q < 0 \end{cases} \tag{47}$$

By substituting Equation (46) in Equation (47), we obtain

$$\begin{cases} s_d \cdot \dot{s}_d = \mathcal{M}_d \left\{ \dfrac{1}{L_g} \dfrac{s_d^2}{\|s_d\| + \alpha} \right\} < 0 \\ s_q \cdot \dot{s}_q = \mathcal{M}_q \left\{ \dfrac{1}{L_g} \dfrac{s_q^2}{\|s_q\| + \alpha} \right\} < 0 \end{cases} \tag{48}$$

Also as the terms $\frac{s_d^2}{\|s_d\|+\alpha}$, $\frac{s_q^2}{\|s_q\|+\alpha}$ and $\frac{1}{L_g}$ are positive, to verify the reaching condition of the controller, the gains $\mathcal{M}_d$ and $\mathcal{M}_q$ must be chosen negative.

4. Simulation results and discussion

Numerical simulations using Matlab/Simulink™ environment are carried out in order to confirm and compare the performance of the proposed scheme. The specifications are listed in the appendix. The reference voltage of DC-link is fixed at 220 V. The reference current i_{qg}^* is set to zero (injecting only the active power). Tests are performed under fast and linear solar irradiation changes as shown in Figure 8 and a fixed temperature of 25 °C. Finally, the proposed control scheme is compared with the conventional scheme (PI based controller), with the same specifications in appendix to provide a fair comparison.
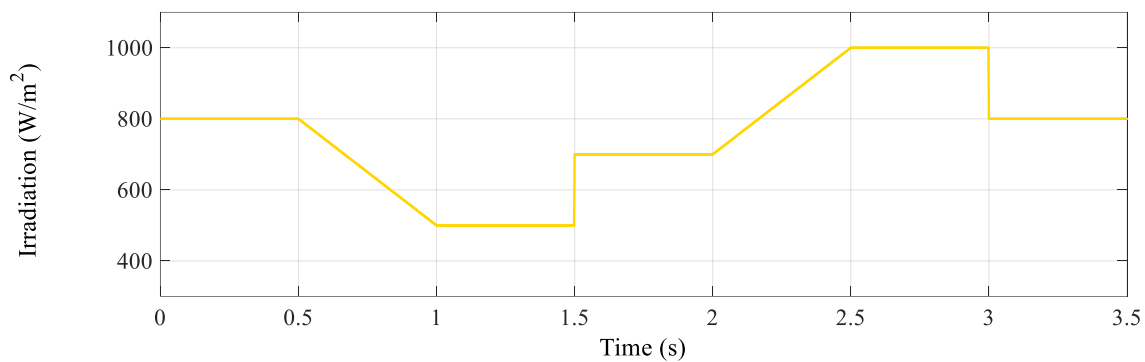
Figure 8. Solar irradiation profile

Figures 9 and 10 represent the results obtained with the conventional and proposed control schemes respectively. From top to bottom, the waveforms given in Figures 9 and 10 are: (a) PV voltage, (b) PV current, (c) PV power, (d) DC-Link voltage with its desired reference, (e) i_{dg} -current with its reference, (f) i_{qg} current with its reference.

At the outset, the results confirm the low tracking speed of the conventional scheme (PI based controller) under irradiation changes with significant PV voltage fluctuation in steady state. In contrast, a high tracking performance was exhibited by using the proposed scheme. Also, an instantaneous effect on the PV voltage is displayed under irradiation changes without overshoots and with less fluctuation, as shown in Figure 11. Due to the relationship between the PV power and PV voltage, the performance of MPP tracking is affected by the PV voltage behavior, when the voltage fluctuation and tracking time are small, the power loss is too. Moreover, Figure 12 illustrates the performance improvement with the proposed scheme compared to the conventional VO-MPPT. For more details, the main simulation results obtained for both MPPT methods are summarized in Table 1.

Table 1. Comparison results for MPPT methods.

MPPT Technique	Step change in irradiation 500→700W/m²		Step change in irradiation 1000→800W/m²		Linear changes in irradiation 800→500W/m² and 700→1000W/m²
	Power oscillation (W)	Response time (s)	Power oscillation (W)	Response time (s)	Tracking accuracy
Conventional VO-MPPT	0.17	0.022	0.23	0.02	low
Proposed VO-MPPT	Less than 0.03	0.0085	0.051	0.0061	Very good

Furthermore, we examine the DC-Link voltage regulation using the conventional PI controller and proposed ISM based scheme. The obtained results shown in Figure 13 confirm the tracking superiority of the proposed scheme compared to the conventional one under any type of irradiation changes. It can be observed, that by using the conventional PI controller, the DC-Link voltage deviates from the reference with a steady state error in case of linear changes in solar irradiation. Moreover, in case of step irradiation changes, the overshoot and response time are significantly large. In contrast, the desired reference is accurately tracked by employing the proposed scheme in addition to insignificant overshoot and short response time under step irradiation changes. To show the performance improvement using the proposed control scheme compared to conventional scheme, key results are presented in Table 2.

Table 2. Comparison results for DC-Link regulation.

Control scheme	linear change in irradiance 800→500 W/m²	Step change in irradiance 500→700 W/m²		linear change in irradiance 700→1000 W/m²	Step change in irradiance 1000→800 W/m²	
	Static error average (%)	Overshoot (%)	Settling time (s)	Static error average (%)	Overshoot (%)	Settling time (s)
Conventional PI	1.512	6.95	0.175	1.478	7.47	0.179
Proposed scheme	0.051	2.2	0.035	0.057	2.98	0.08

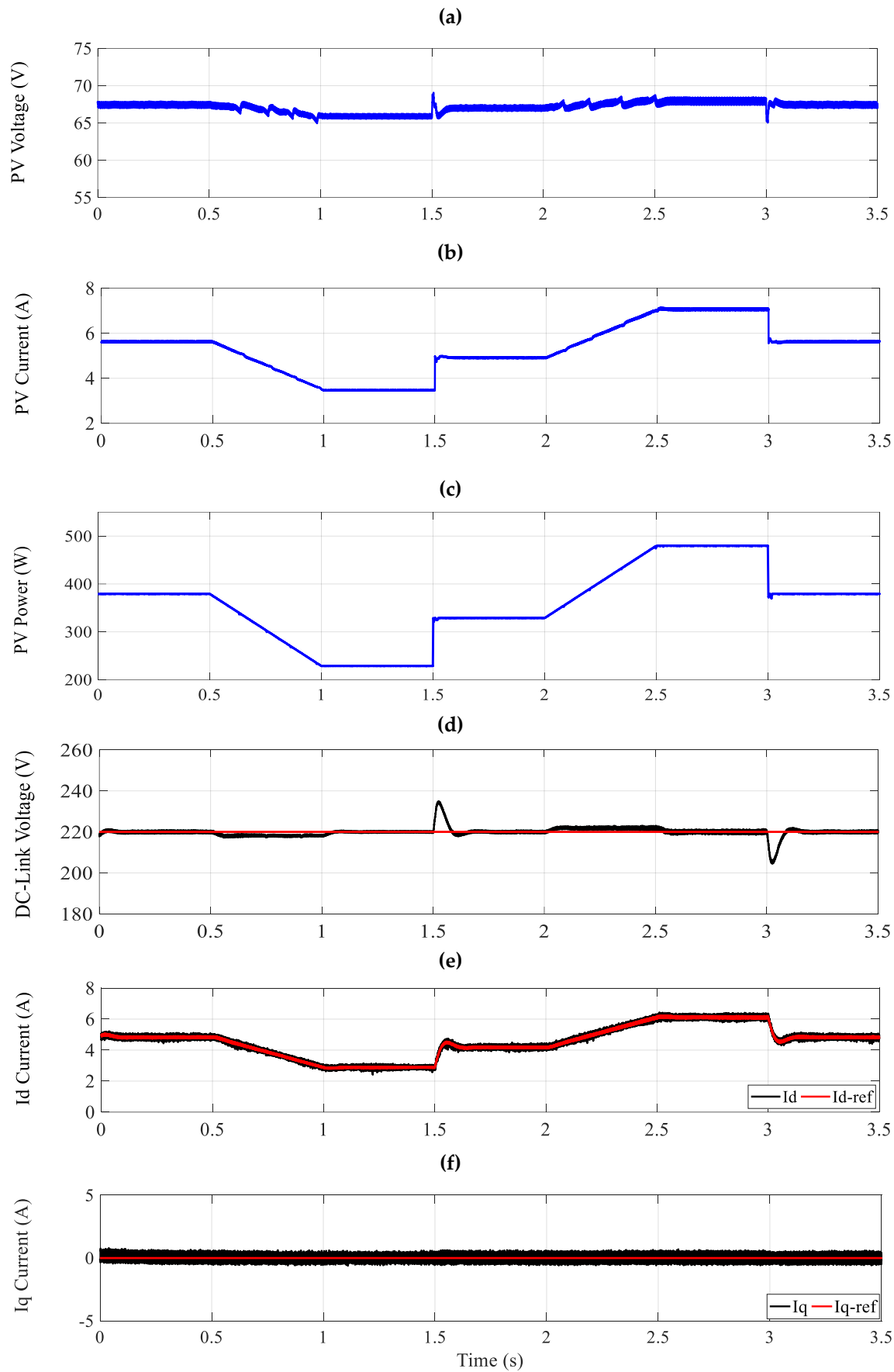**Figure 9.** Simulation results of the grid-tied PV system with the conventional control scheme under irradiation changes.

(a)
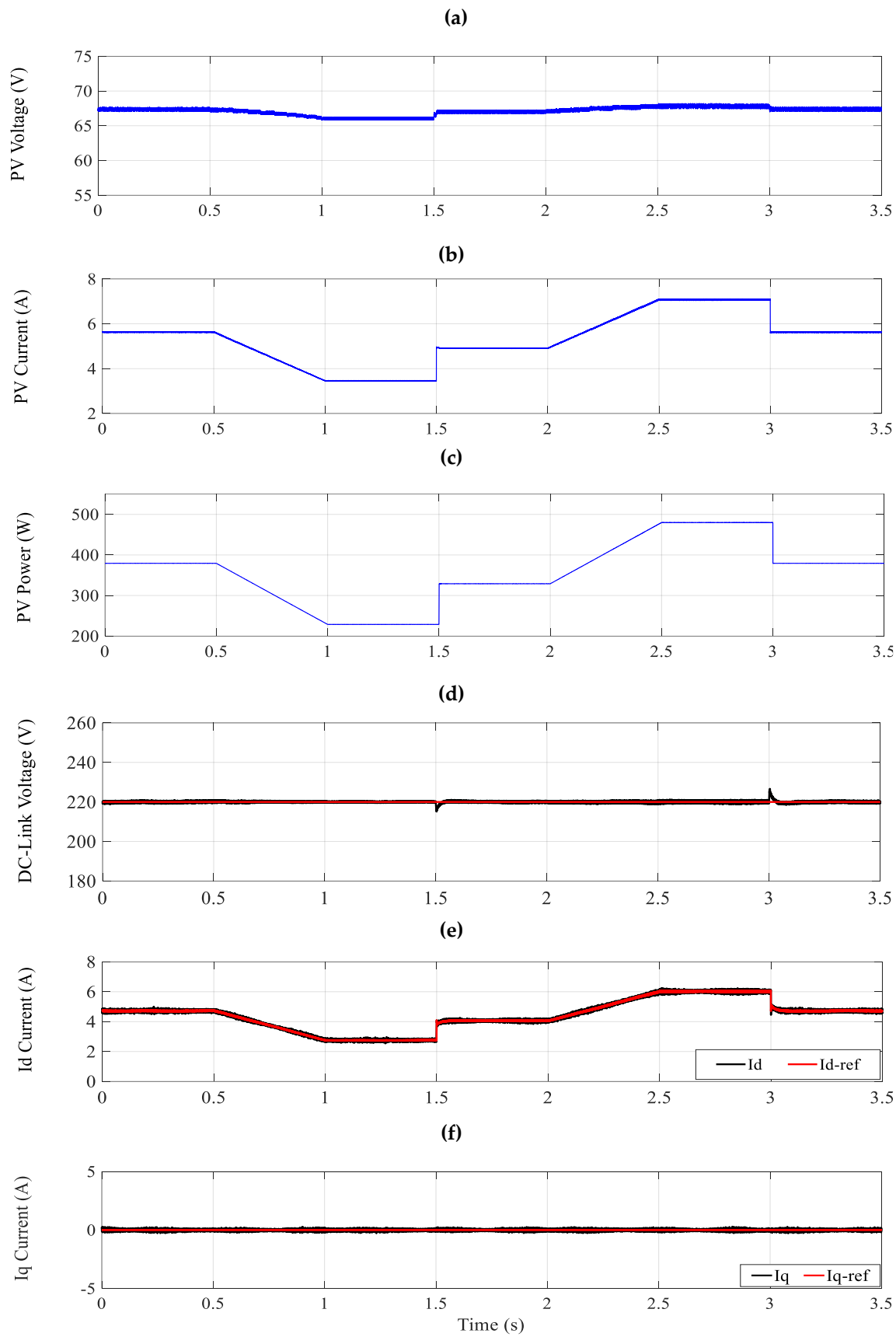
(b)

(c)

(d)

(e)

(f)

Figure 10. Simulation results of the grid-tied PV system with the proposed control scheme under irradiation changes.
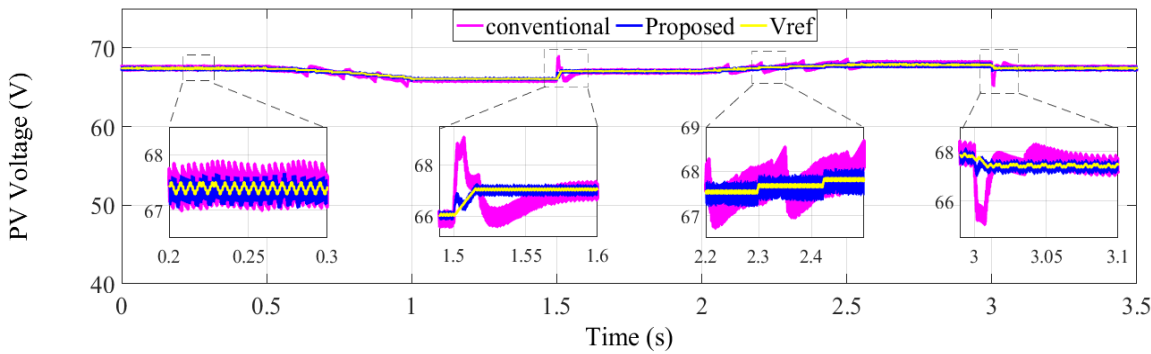
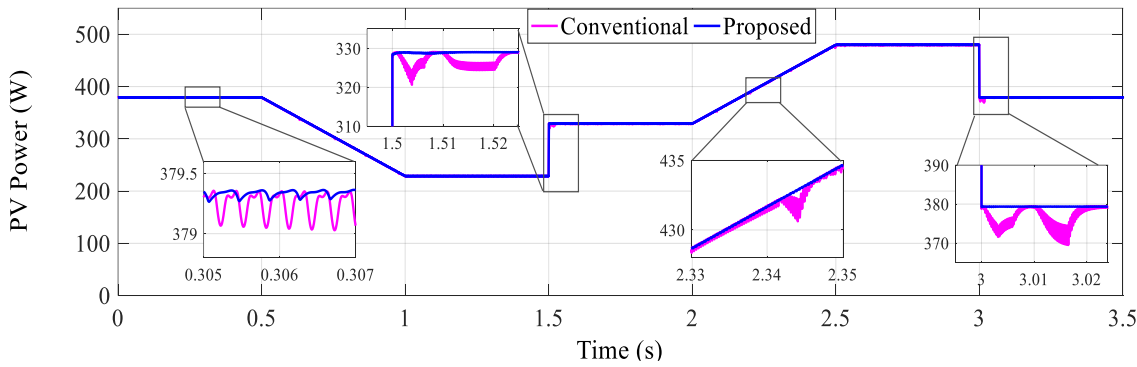**Figure 11.** Simulated PV Voltage with conventional and proposed VMPPT methods

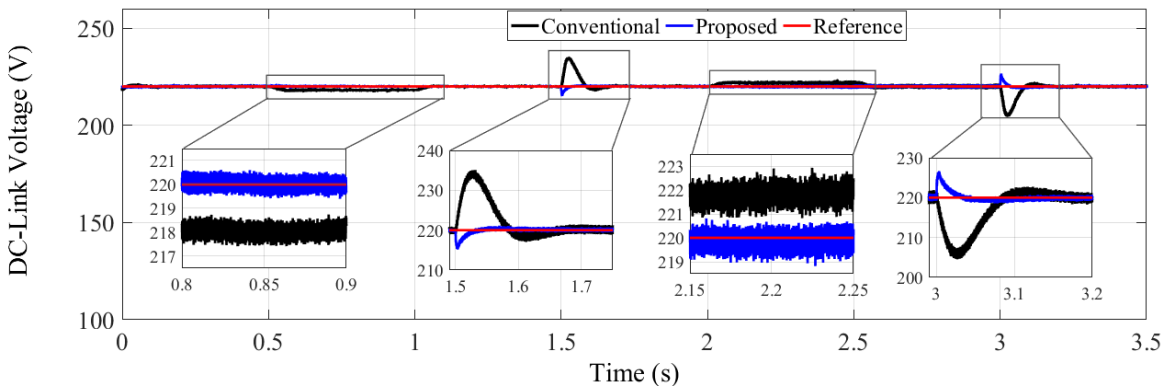**Figure 12.** Simulated PV Power with conventional and proposed VMPPT methods

Figure 13. DC-Link voltage response with conventional and proposed methods

We also observe that the proposed VOC-ISM scheme injects the extracted PV power into the grid with high quality and efficiency, contrary to the conventional scheme (VOC-PI controller). It can be observed that i_{dg} and i_{qg} currents are completely regulated to their references in the proposed scheme. It is found that i_{dg} current exhibits fast response with less fluctuation compared to the conventional control, as shown in Figure 10e,   which leads to grid currents of good quality and almost instantaneously follow the irradiation changes, as shown in Figure 14b. In contrary, the grid currents waveforms in the conventional scheme are relatively of poor quality due to the large fluctuation and response time of i_{dg} current, as shown in Figure 14a. A comparison summary in terms of key indexes such as grid current THD and i_{dg} current ripples for various irradiation levels is depicted in Figure 15.
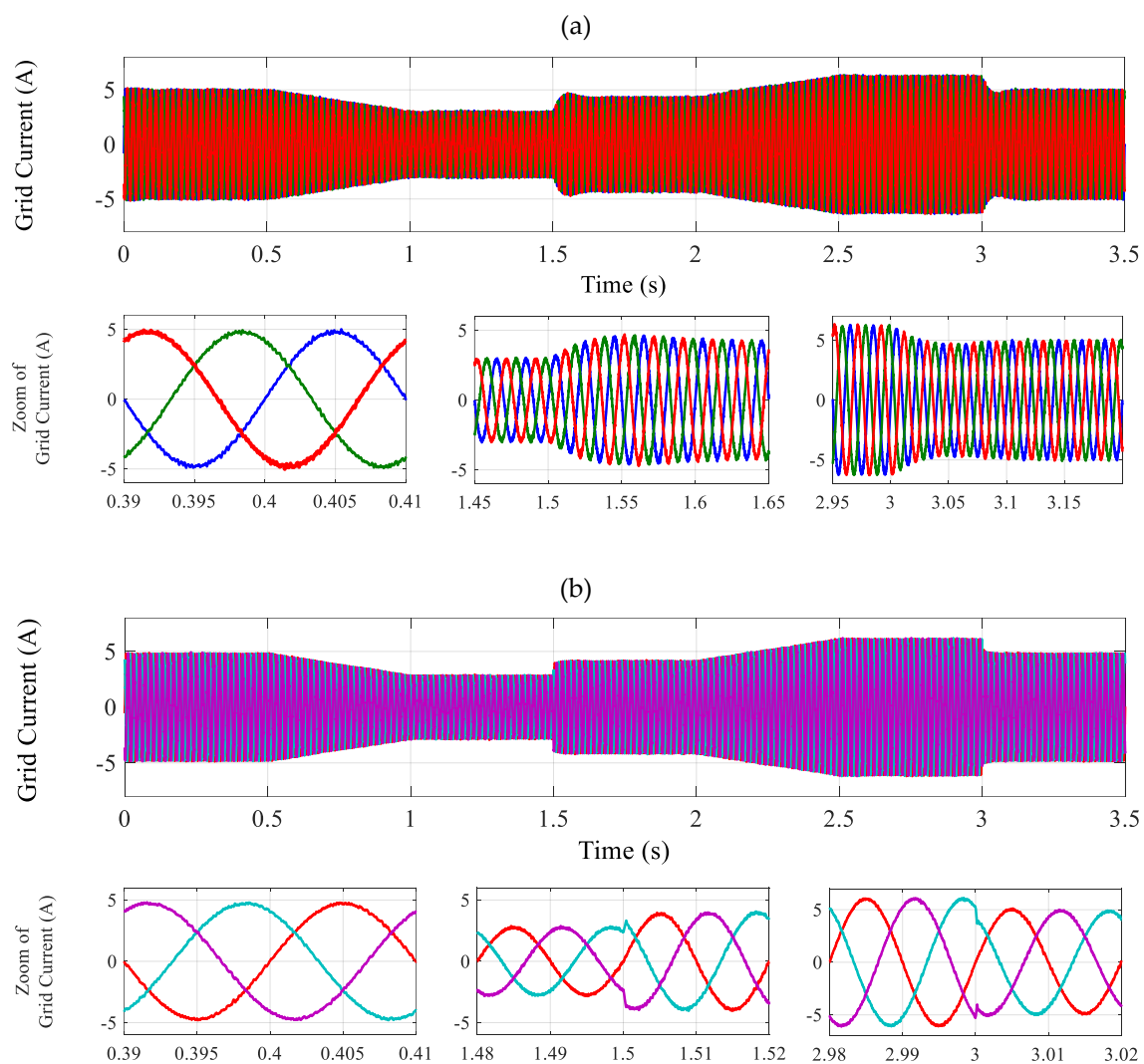

Figure 14. Grid currents with zoom waveforms for (a) conventional and (b) proposed schemes under irradiation changes.
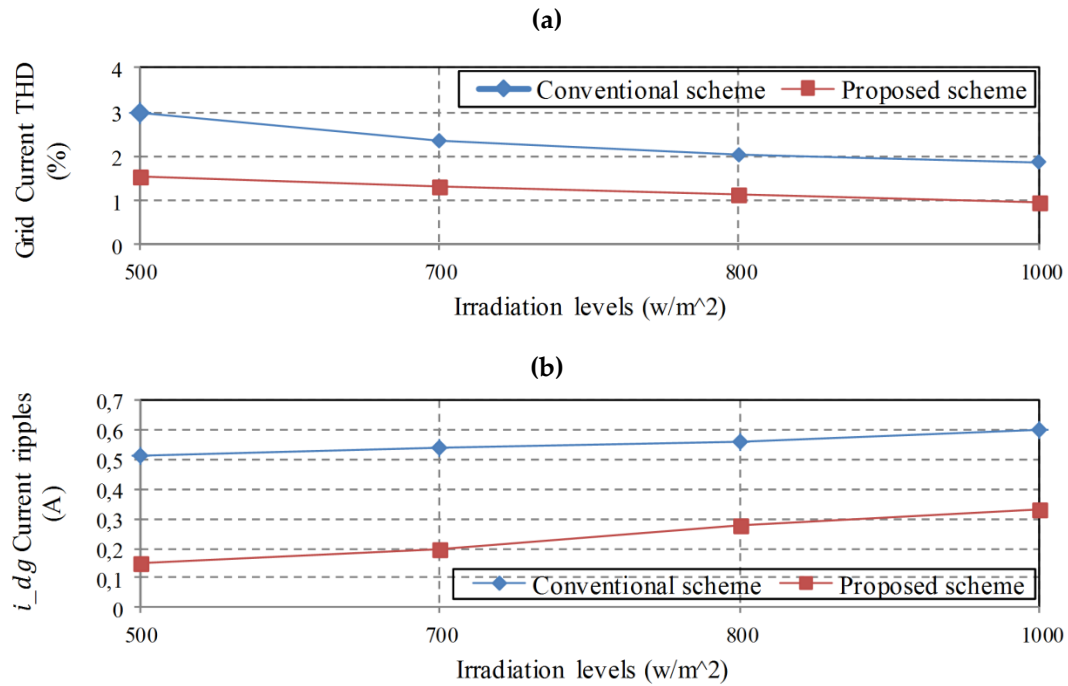
(a)

(b)

Figure 15. Grid current quality under irradiation changes

5. Conclusion

This paper proposed a high performance control scheme for two-stage grid-tied PV system. The control structure of the proposed scheme is based on ISMC theory and consists of MPPT control, DC-Link voltage regulation loop, and VOC based on inner current control loops to improve system performance during all climatic conditions.   As it is a two stage system, the PV power is provided to the grid through DC-DC boost converter and three phase voltage source inverter.   An ISM controller for boost converter has been proposed for MPP tracking. Moreover, for proper inverter operation as well sinusoidal currents injection into the mains grid with low THD (< 5%), a novel design for DC-Link voltage regulation is suggested to maintain the DC-Link voltage constant at the desired value and estimate the reference currents for VOC scheme, which is based on ISM controllers and space vector modulator. The simulation results obtained confirm the feasibility, effectiveness and performance improvement of the proposed control scheme.

Author Contributions: A.K. and B.T. designed and achieved the method; F.K. verified and analyzed the results; A.L. and A.S. wrote the paper.

Conflicts of Interest: The authors declare no conflict of interest.

Appendix

The global specifications of the grid-tied PV system used in the simulation are listed in Table 3.

Table 3. Global system specifications.

GPV	Nominal values
Open circuit voltage (V_{OC})	42.1 [V]
Optimum operating voltage(V_{mpp})	33.7 [V]
Short circuit current (I_{SC})	3.87 [A]
Optimum operating current (I_{mpp})	3.56 [A]
Maximum power (P_{mpp})	120 [W]
Number of cells connected in seriesN_s	72
Number of cells connected in parallel N_p	1
Number of panels connected in series N_{ss}	2
Number of panels connected in parallel N_{pp}	2
Boost converter	**Value**
Inductance (L)	1 [mH]
Input capacitor (C_{in})	470 [μF]
output capacitor (C_{dc})	200 [μF]
Electrical parameters of grid-tied	**value**
Output filter inductance (L_g)	10 [mH]
Line resistance (R_g)	0.1 [Ω]
Nominal grid frequency (f_g)	50 [Hz]
Nominal line voltage of the 3-phase grid (v_g)	100 [V]
Simulation parameters	**value**
VMPPT sampling frequency (T_s)	1 [kHz]
PWM switching frequency ($f_{s,PWM}$)	5 [kHz]
SVM switching frequency ($f_{s,SVM}$)	25 [kHz]

References

1. Dincer, F. The analysis on photovoltaic electricity generation status, potential and policies of the leading countries in solar energy. *Renew. Sustain. Energy Rev.* **2011**, 15, 713-720.
2. Shayestehfard, A.; Mekhilef, S.; Mokhlis, H. IZDPWM based feed forward controller for grid connected inverters under unbalanced and distorted conditions. *IEEE Trans. Ind. Electron.* **2017**, 64, 14-21.
3. Xiao, W.; Edwin, F.F.; Spagnuolo, G.; Jatskevich, J. Efficient approaches for modeling and simulating photovoltaic power systems. *IEEE J. Photovolt.* **2013**, 3, 500-508.
4. Kanaan, H.; Caron, M.; Al-Haddad, K. Design and implementation of a two-stage grid-connected high efficiency power load emulator. *IEEE Trans. Power Electron.* **2014**, 29, 3997-4006.
5. Debnath, D.; Chatterjee, K. Two-stage solar photovoltaic-based stand-alone scheme having

battery as energy storage element for rural deployment. _IEEE Trans. Ind.   Electron_. **2015**, 62, 4148-4157.

6. Femia, N.; Petrone, G.; Spagnuolo, G.; Vitelli, M. Power electronics and control techniques for maximum energy harvesting in photovoltaic systems. CRC Press **2012**.

7. Ahmed, J.; Salam, Z. An improved perturb and observe (P&O) maximum power point tracktwotwing (MPPT) algorithm for higher efficiency. _Appl. Energy_ **2015**, 150, 97-108.

8. De Brito, M.A.G.; Galotto, L.; Sampaio, L.P.; Melo, G.D.A.; Canesin, C.A. Evaluation of the main MPPT techniques for photovoltaic applications. _IEEE Trans. Ind. Electron._ **2013**, 60,1156–1167.

9. Safari, A.; Mekhilef, S. Simulation and hardware implementation of incremental conductance MPPT with direct control method using cuk converter. _IEEE Trans. Ind. Electron_. **2011**, 58,1154–1161.

10. Belkaid, A.; Colak, I.; Isik, O. Photovoltaic maximum power point tracking under fast varying of solar radiation. _Appl. Energy_ **2016**, 179,523-530.

11. Rizzo S.A.; Scelba, G. ANN based MPPT method for rapidly variable shading conditions. _Appl. Energy_ **2013**, 145,124-132.

12. Karatepe, E.; Hiyama, T. Artificial neural network-polar coordinated fuzzy controller based maximum power point tracking control under partially shaded conditions. _IET Renew. Power Gener_. **2009**, 3, 239-253.

13. Al Nabulsi, A.; Dhaouadi, R. Efficiency optimization of a DSP-based standalone PV system using fuzzy logic and dual-MPPT control. _IEEE Trans. Ind. Informa_. **2012**, 8, 573-584.

14. Zainuri, M.A.A.M.; Radzi, M.A.M.; Soh, A.C.; Abd Rahim, N. Development of adaptive perturb and observe-fuzzy control maximum power point tracking for photovoltaic boost dc–dc converter. _IET Renew. Power Gener_. **2014**, 8, 183-194.

15. Bendib, B.; Belmili, H.; Krim, F. A survey of the most used MPPT methods: Conventional and advanced algorithms applied for photovoltaic systems. _Renew. Sustain. Energy Rev_. **2015**, 45, 637-648.

16. Shaiek, Y.; Smida, M.B.; Sakly, A.; Mimouni, M.F. Comparison between conventional methods and GA approach for maximum power point tracking of shaded solar PV generators. _Sol. Energy_ **2013**, 90, 107-122.

17. Ishaque, K.; Salam, Z.; Amjad, M.; Mekhilef, S. An improved particle swarm optimization (PSO)–based MPPT for PV with reduced steady-state oscillation. _IEEE Trans. Power Electron_. **2012**, 27, 3627-3638.

18. Mohanty, S.; Subudhi, B.; Ray, P.K. A new MPPT design using grey wolf optimization technique for photovoltaic system under partial shading conditions. _IEEE Trans. Sustain.   Energy_ **2016**, 7, 181-188.

19. Bianconi, E.; Calvente, J.; Giral, R.; Mamarelis, E.; Petrone, G.; Ramos-Paja, C.A.; Spagnuolo, G.; Vitelli, M. A fast current-based MPPT technique employing sliding mode control. _IEEE Trans. Ind. Electron_. **2013**, 60, 1168-1178.

20. Kakosimos, P.E.; Kladas, A.G.; Manias, S.N. Fast photovoltaic-system voltage-or current-oriented MPPT employing a predictive digital current-controlled converter. _IEEE Trans. Ind. Electron_. **2013**, 60, 5673-5685.

21. Elgendy, M.A.; Zahawi, B.; Atkinson, D.J. Assessment of perturb and observe MPPT algorithm implementation techniques for PV pumping applications. _IEEE Trans. Sustain. Energy_ **2012**, 3, 21-33.

22. Pradhan, R.; Subudhi, B. Double integral sliding mode MPPT control of a photovoltaic system. _IEEE Trans. Cont. Syst. Technology_ **2016**, 24, 285-292.

23. Farhat, M.; Barambones, O.; Sbita, L. A new maximum power point method based on a sliding mode approach for solar energy harvesting. _Appl.Energy_ **2017**, 185,1185–1198.

24. Talbi, B.; Krim, F.; Rekioua, T.; Mekhilef, S.; Laib, A.; Belaout, A. A high-performance control scheme for photovoltaic pumping system under sudden irradiance and load changes. _Sol. Energy_ **2018**, 159, 353-368.

25. Menadi, A.; Abdeddaim, S.; Ghamri, A.; Betka, A. Implementation of fuzzy-sliding mode based

control of a grid connected photovoltaic system. *ISA Trans.* **2015**, 58, 586-594.

26. Vitorino, M.A.; de Rossiter, C.M.B.; Jacobina, C.B.; Lima, A.M.N. An effective induction motor control for photovoltaic pumping. *IEEE Trans. Ind. Electron.* **2011**, 58, 1162-1170.

27. Achour, A.; Rekioua, D.; Mohammedi, A.; Mokrani, Z.; Rekioua, T.; Bacha, S. Application of direct torque control to a photovoltaic pumping system with sliding-mode control optimization. *Electric Power Compon. Syst.* **2016**, 44, 172-184.

28. Hu, J.; Zhu, Z.Q. Investigation on switching patterns of direct power control strategies for grid-connected DC–AC converters based on power variation rates. *IEEE Trans. Power Electron.* **2011**, 26, 3582-3598.

29. Malinowski, M.; Kazmierkowski, M.P.; Hansen, S.; Blaabjerg, F.; Marques, G.D. Virtual-flux-based direct power control of three-phase PWM rectifiers. *IEEE Trans. Ind. Appl.* **2001**, 37, 1019-1027.

30. Jain, C.; Singh, B. A three-phase grid tied SPV system with adaptive DC link voltage for CPI voltage variations. *IEEE Trans. Sustain. Energy* **2016**, 7, 337-344.

31. Rodriguez, J.; Pontt, J.; Silva, C.A.; Correa, P.; Lezana, P.; Cortés, P.; Ammann, U. Predictive current control of a voltage source inverter. *IEEE Trans. Ind. Electron.* **2007**, 54, 495-503.

32. Teodorescu, R.; Liserre, M.; Rodriguez, P. Grid converters for photovoltaic and wind power systems. *John Wiley & Sons.* **2011**, 29.

33. Utkin, V.I. Sliding mode control design principles and applications to electric drives. *IEEE Trans. Ind. Electron.* **1993**, 40, 23-36.

34. Edwards, C.; Spurgeon, S. Sliding mode control: theory and applications. CRC Press **1998**.

35. Tan, S.C.; Lai, Y.M.; Tse, C.K. Sliding mode control of switching power converters: techniques and implementation. CRC Press **2011**.

36. Sebaaly, F.; Vahedi, H.; Kanaan, H.Y.; Moubayed, N.; Al-Haddad, K. Sliding mode fixed frequency current controller design for grid-connected NPC inverter. *IEEE J. Emerg. Slect. Top. Power Electron.* **2016**, 4, 1397-1405.

37. Van Dijk, E.; Spruijt, J.N.; O'sullivan, D.M.; Klaassens, J.B. PWM-switch modeling of DC-DC converters. *IEEE trans. Power Electron.* **1995**, 10, 659-665.

38. Utkin, V.; Guldner, J.; Shi, J. Sliding mode control in electro-mechanical systems. CRC Press **2009**.

39. Hamayun, M.T.; Edwards, C.; Alwi, H. Fault tolerant control schemes using integral sliding modes. *Springer Inter. Publishing*; **2016**.

40. Yaramasu, V.; Wu, B.; Chen, J. Model-predictive control of grid-tied four-level diode-clamped inverters for high-power wind energy conversion systems. *IEEE trans. Power Electron.* **2014,** 29, 2861-2873.